Time-resolved PIV Measurement of a Developing Zero Pressure Gradient Turbulent Boundary Layer

J. H. Lee, Y. S. Kwon, J. P. Monty and N. Hutchins

Department of Mechanical Engineering, The University of Melbourne, Victoria 3010, Australia.

Abstract

Time-resolved two-dimensional particle image velocimetry (TR-PIV) is employed to measure the instantaneous velocity fields in an evolving zero-pressure-gradient (ZPG) turbulent boundary layer. The spatially developing boundary layer is formed on a flat plate which is towed past a stationary time-resolved PIV system such that each pass yields streamwise/wall-normal planes of data with Reynolds numbers in the range $500 \lesssim Re_\tau \lesssim 2500$. This provides a unique view of a spatially and temporally evolving turbulent boundary layer from the tripwire up to high Reynolds numbers. In this frame of reference an evolving large-scale structure, with a convection velocity close to the freestream, appears nominally stationary within the field of view. This system is effectively equivalent to moving an entire PIV system with the flow, chasing the large-scale structures as they advect downstream in a wind tunnel or a water channel facility [8]. Complete instantaneous velocity vector fields of such a developing turbulent boundary layer provide clearer insight into the mechanisms associated with large-scale coherent structures in the outer region of turbulent boundary layers. The mean flow parameters of the experimental data are assessed to evaluate the quality of the turbulent boundary layers formed on the towed-plate. These results indicate that the developing turbulent boundary layer in this study can be considered 'canonical' with a nominally zero-pressure-gradient. An analysis of instantaneous convection velocities associated with low- and high-speed structures reveals differences in the trajectory and local convection velocity of these features as the turbulent boundary layer develops along the flat plate.

Facility and Experimental Setup

Experiments are performed in the tow tank facility located in the Michell hydrodynamics laboratory at the University of Melbourne. The tow tank has dimensions of $60 \times 2 \times 2$ m (length $\times$ width $\times$ height) and is filled with water. The tow tank facility has a computer controlled traversing carriage that can tow models at various speeds of up to 2.5 m/s. A 5.0 m long and 1.2 m wide flat plate is suspended horizontally beneath the traversing carriage by four aerofoil shaped supports. The height of the supports can be individually adjusted so that the pressure gradient along the plate can be controlled. The bottom side of the plate is positioned 10 mm below the water surface. The test surface of the flat plate consists of black anodised aluminium sheets. The leading edge of the plate consists of an 8:1 ratio semi-elliptical nose to prevent a flow separation. A schematic of the tow tank facility and the flat plate setup are shown in figure 2. A 1.0 mm diameter trip wire is located immediately downstream of the leading edge to stimulate the boundary layers formed on the bottom surface of the plate. The Reynolds number of the trip based on the diameter of the wire is $Re_d = dU_\infty/\nu \approx 870$ (where U_∞ is plate velocity, d is trip wire diameter and ν is kinematic viscosity) at a given plate velocity of approximately 1.0 m/s. This Re_d is comparable with recommendations from previous studies [7]. The carriage is fully automated such that multiple passes can be performed to obtain converged statistics of the developing turbulent boundary layers. Figure 1 shows variation of the background turbulence intensity as a function of time between each pass of the towed plate. The result reveals that at least $8 \sim 10$ minutes are required to allow the
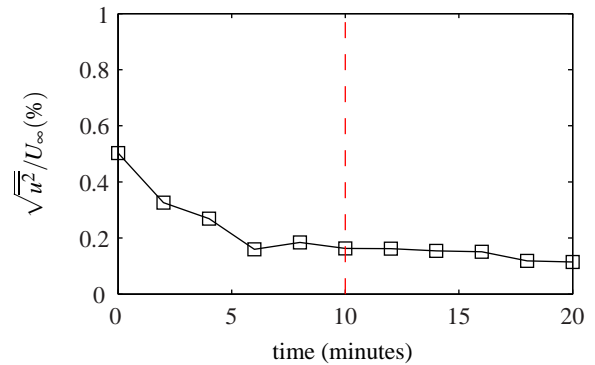

Figure 1. Variation of background turbulence intensity in time between measurements. The broken line indicates the time required between measurements

water to settle ($\sqrt{\overline{u^2}}/U_\infty < 0.2\%$) between passes. Preliminary non time-resolved PIV experiments show that approximately 800 image pairs are required to obtain converged turbulence intensity $\overline{u^2}$. Therefore, the total measurement time required to obtain the converged statistics equates to approximately 150 hours. We note that this is only possible with a fully automated measurement system. In order to automate the carriage, an encoder is integrated on the carriage, measuring the local velocity and position of the carriage during the measurements. A micro-epsilon opto NCDT ILR-1182 laser range finder (error range of $\pm$ 2 mm over 150 m) is installed at the downstream end of the tank and targeted on the carriage to independently measure the absolute position of the carriage relative to the tank, providing a separate measure of the carriage velocity. A PID feedback control algorithm is implemented along with the traversing carriage controller to maintain a carriage velocity deviation within $\pm 0.5\%$ during the experiment. Underwater optical access is provided through viewing windows located 25 m from the upstream end of the tank. The stationary image acquisition system including a laser, cameras and optics is placed in front of the viewing windows to acquire a set of time-resolved images as the plate is towed past. Throughout this paper, x, y and z denote the streamwise, spanwise and wall-normal directions, respectively. Overbars indicate time-averaged quantities (e.g. $\overline{u}$). The superscript '+' is used to denote quantities normalised by viscous scaling (e.g. $z^+ = zu_\tau/\nu$, $U^+ = U/u_\tau$ and $t^+ = tu_\tau^2/\nu$). The PIV setup consists of a Photonics DM20-527 dual head Nd:YLF laser that delivers 100 mJ/pulse at 1000 Hz, and two PCO Dimax CMOS cameras with 32GB buffer. The cameras have a resolution of 2000×2000 pixels and a bit depth of 12 bits. Two cameras are located side-by-side providing an elongated field of view in the streamwise direction of 170×80 mm ($x \times z$). Both cameras use a Tamaron f/3.5 180 mm macro lens and the object distance between the camera sensor plane and the light sheet is approximately 1000 mm. The laser sheet has a thickness of approximately 1.5 mm, illuminating an $x - z$ plane (streamwise/wall-normal) along the centre line of the flat plate. The tank is seeded with hollow glass spheres with a mean diameter of 10 μm. All images are acquired at a sampling rate of 1000 Hz which gives $\Delta t = 1$ ms (where Δt is the time between
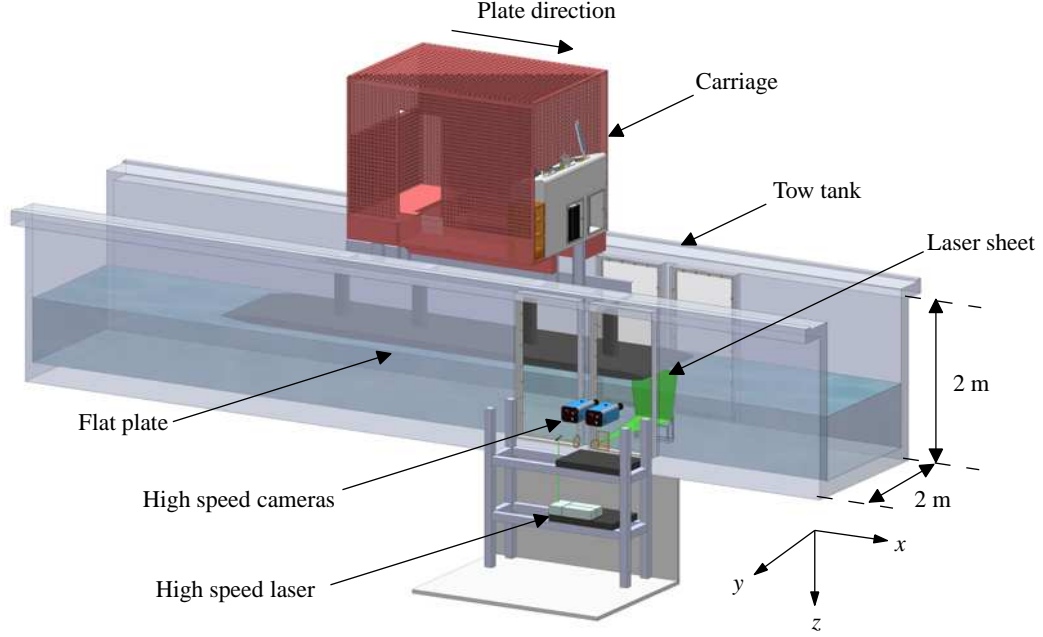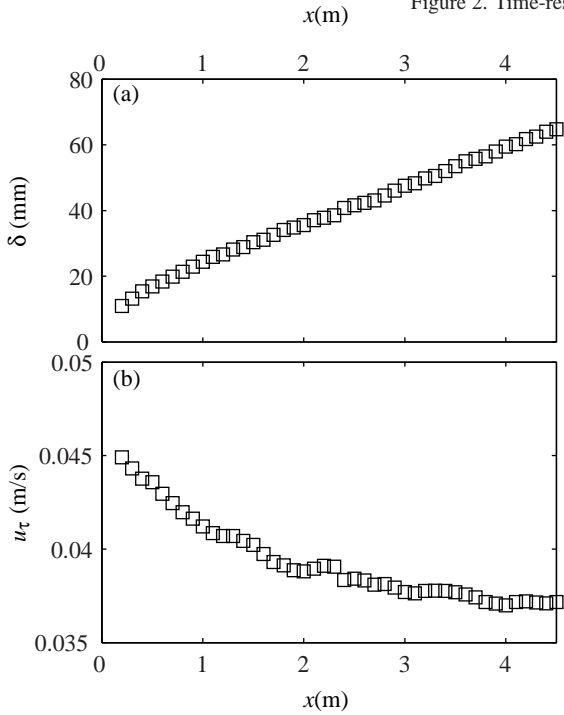
Figure 2. Time-resolved PIV setup in the tow tank

Figure 3. (a) Growth of boundary layer thickness (δ) and (b) Friction velocity (u_τ) as a function of the streamwise distance from the trip wire

.

images) for a sampling time of 5.0 s. This equates to $\Delta t^+ \approx 1.53$ for $U_\infty = 1$ m/s. The schematic of the tow tank experiment with time-resolved PIV setup is shown in figure 2. A total of 122 runs are performed and each run acquires 5000 images to cover the entire streamwise domain of the plate from the trip to the trailing edge ($0 \lesssim x \lesssim 5$ (m)). The obtained images are processed using an in-house PIV package. A final interrogation window size of 32×32 pixels and a 50 % overlap are employed for all measurements yielding a spatial resolution of $58 \times 58 \times 60$ wall units for the interrogation volume. Processed velocity vector fields are stitched based on calibration images obtained from imaging an *in situ* calibration target. Further details on the PIV processing algorithm and calibration are available in de Silva *et al.* [6]. Since the turbulent boundary layer is continually developing as the plate is towed past the measurement station, the boundary

layer thickness (δ) and the friction velocity (u_τ) change with x as shown in figure 3. The friction velocity, u_τ, is calculated from a Clauser fit [3] to the mean velocity profile using log law constants $\kappa = 0.41$ and $A = 5.0$. Summarised experimental parameters are shown in Table 1 (where l^+ is the interrogation window size normalised by the viscous length scale and $Re_\tau = \delta u_\tau / \nu$ is the Kármán number).

Carriage velocity (U_∞)	1.0 m/s
Field of view ($x \times z$)	170×80 mm
Laser sheet thickness	1.5 mm ($\approx 60^+$)
Sampling frequency	1000 Hz
Time between laser pulse (Δt)	1 ms ($\Delta t^+ \approx 1.53$)
Pixel size	46 μm
Interrogation window size (pixel)	32×32 ($l^+ \approx 58$)
Range of Reynolds number, Re_τ	$\approx 494 - 2550$

Table 1. Experimental parameters for time-resolved PIV measurement. Since u_τ changes continuously along the plate, mean $\overline{u}_\tau = 0.039$ m/s from figure 3(b) is used to approximate the viscous scaled parameters.

Assessment of Mean Flow Parameters

Mean flow parameters obtained from the current study are evaluated and compared with previously established criteria [1] to assess the quality of the developing turbulent boundary layers. This assessment determines whether the developing turbulent boundary layer can be classified as a '*canonical*' state with a zero pressure gradient, and whether it is approaching the turbulent 'equilibrium' state. Figure 4 shows mean velocity profiles of the developing turbulent boundary layers at various Reynolds numbers (—). It should be noted that the time-resolved PIV measurement yields accurate mean velocity measurements for $z^+ > 100$. The lack of data near the wall is due to measurement issues such as the surface reflection and sparsity of seeding which are known to cause errors in velocity vector fields. Since the mean flow parameters are obtained from the mean velocity profiles, a composite velocity profile (with $\kappa = 0.41$ and $A = 5.0$) proposed by Chauhan *et al.*[1] is used to complete the mean velocity profiles for $z^+ < 100$ and it is plotted on figure 4 using ($\circ$) symbols. Obtaining u_τ from the Clauser method at low Reynolds numbers ($Re_\tau \lesssim 900$) is somewhat unreliable due to the limited log region
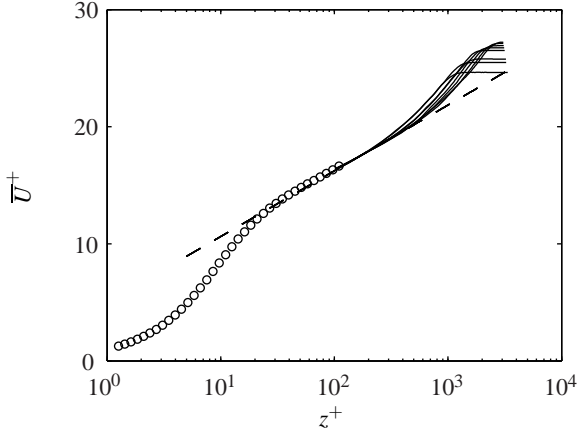
Figure 4. Development of mean velocity profiles with increase in Reynolds number ($800 \lesssim Re_\tau \lesssim 2500$) for developing turbulent boundary layer. ($—$) developing boundary layers, ($- -$) shows $\overline{U}^+ = (1/\kappa)\ln(z^+) + A$ and ($\circ$) shows a composite velocity profile [1] for $z^+ < 100$ (where $\kappa = 0.41$ and $A = 5.0$)

in the mean velocity profiles. $Re_\tau \approx 900$ is obtained 1 m downstream of the trip. This distance is still relatively 'close' to the initial tripping condition and these low Reynolds numbers have limited scale separation between the near-wall and log region. For reference, this limit ($x = 1$m, $Re_\tau= 900$) is shown on figure 5 by the red dashed lines. The shape factor, $H = \delta^*/\theta$ (where δ^* and θ are the displacement thickness and the momentum thickness, respectively), the skin friction coefficient, c_f and the wake factor, Π, are computed to evaluate the quality of the developing boundary layers in this study. To compute H for the experimental data, the mean velocity profiles completed with the composite velocity profile shown in figure 4 are used. The variation of H for the developing boundary layer as Reynolds number increases is shown in figure 5(a). In an effort to ease comparability with previous studies [1, 10], $Re_\theta = \theta U_\infty/\nu$ is plotted on the bottom abscissa in figure 5. The solid line indicates H computed from the composite profile [1] and the dashed lines show a 1 % tolerance. The discrepancy observed in the low Reynolds number region ($Re_\theta \lesssim 2500$) could be due to the proximity to the trip. However, it is worth noting that the trend of H is in good agreement with previously published data in the higher Reynolds number region. The variation of skin friction coefficient c_f as Reynolds number increases is plotted and compared with the Coles-Fernholz relationship in figure 5(b). There is some error associated with calculating c_f from the Clauser method. Nevertheless, the scatter of data in figure 5(b) lie within ± 5 % tolerance and the general trend is in good agreement with the Coles-Fernholz relationship. The wake factor Π is an indication of whether a turbulent boundary layer is correctly stimulated for a given tripping condition. Π is obtained using the relationship $\Delta \overline{U}/u_\tau = 2\Pi/\kappa$ (see [4]), where $\Delta \overline{U}/u_\tau$ is the maximum deviation between a mean velocity profile and the log law, and $\kappa = 0.41$. The evolution of Π with Reynolds number for the developing turbulent boundary layer is shown in 5(c). Collins et al.[5] data is included for a comparison. The disparity in the low Reynolds number region shown in figure 5(c) could be caused by the different trip conditions. However, it is noted that Π seems to approach an asymptotic value as Reynolds number increases which is previously reported in the literature [4, 7].

Convection Velocity Analysis

Preliminary analysis on the convection velocity of low- and high-speed structures is presented in this section. Figure 6 shows the normalised streamwise fluctuating velocity field ($u/\overline{u}_\tau$) at $z = 0.15\delta$ in the $x - t$ plane, offering a unique view of the convected instantaneous velocity fluctuation signature associated with low- and high-speed structures. To maintain the fixed wall-
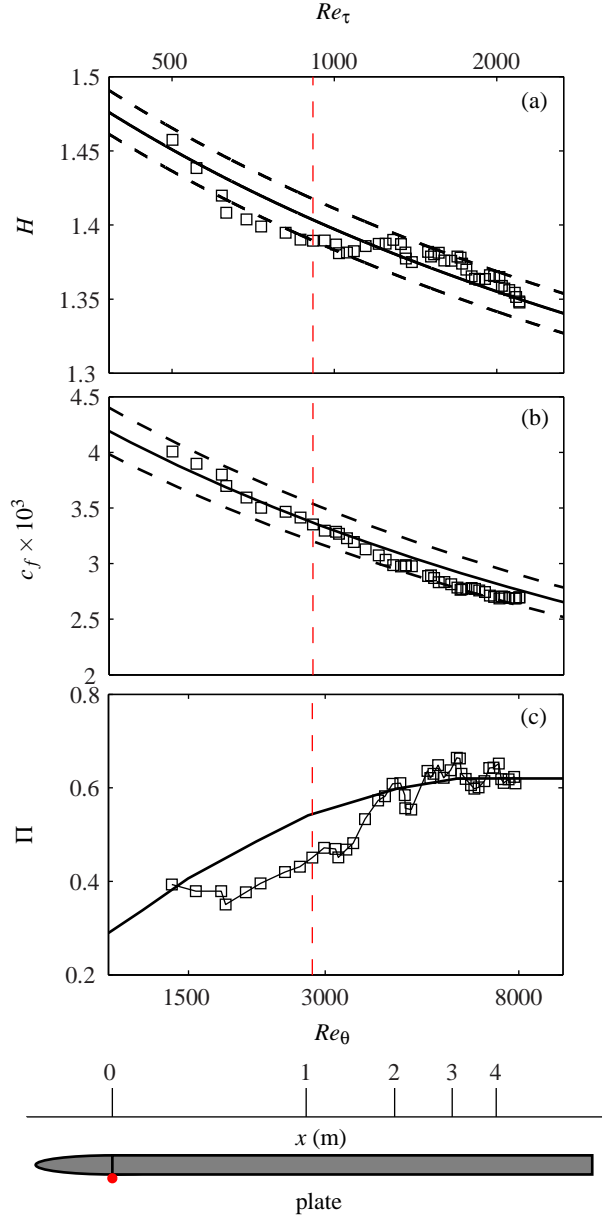

Figure 5. (a) Shape factor, H, for developing boundary layer as function of Reynolds number. ($—$) is the integration of composite profile [1] and ($- -$) shows a 1% tolerance. (b) Skin-friction coefficient, c_f, as function of Reynolds number. ($—$) represents Coles-Fernholz relation, $c_f = 2((1/\kappa)\ln(Re_\theta) + A)^{-2}$, and ($- -$) is a 5% tolerance (with $\kappa = 0.41$ and $A = 5.0$). (c) Wake factor, Π, with Reynolds number. ($—$) is data from Collins et al. [5]

position in terms of δ ($z = 0.15\delta$), the z location of the data shown in figure 6 increases from left to right. Blue shading represents low-speed structures and red represents high-speed. Inclined striped features shown in figure 6 indicate trajectories of the structures in x and with time, t, as the turbulent boundary layer develops. These features reveal convection velocities of low- and high-speed structures by detecting an inclination angle of the stripes. Only the regions with the velocity fluctuation magnitude greater than $\overline{u}_\tau$ are included in the analysis ($|u| > \overline{u}_\tau$). Once the features are identified, an ellipse is fitted to each feature and the major axis of the ellipse indicates the corresponding inclination angle of the feature as shown in figure 6. The dot-dashed lines represent the major axes of the fitted ellipses (where θ_l and θ_h are the inclination angles of low- and high-speed features, respectively). The convection velocity of the low-speed and the high-speed regions ($U_{c,l}$ and $U_{c,h}$, respectively) can then
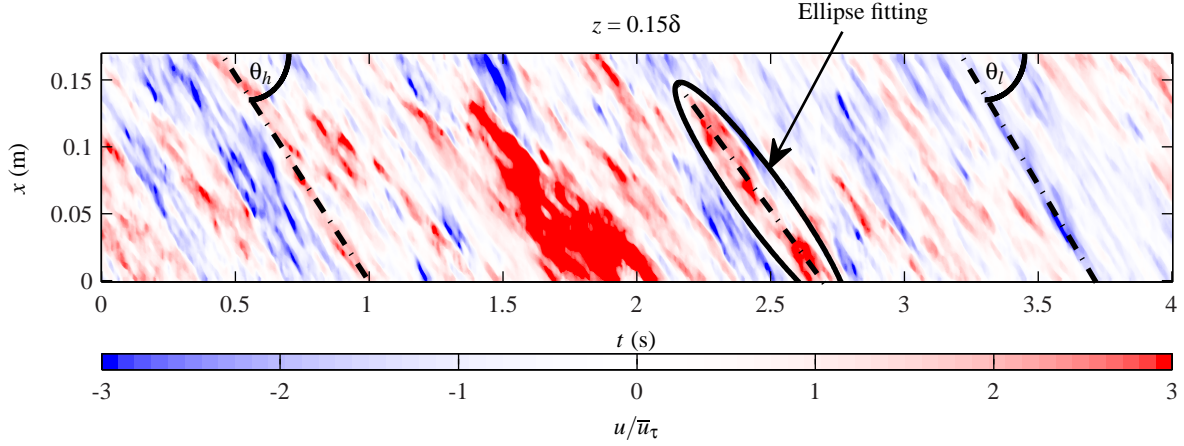
Figure 6. Normalised streamwise fluctuating velocity field ($u/\overline{u}_\tau$) at $z = 0.15\delta$ in $x - t$ plane. Dot-dashed lines show detected inclination angle of striped features.

be computed from the inclination angle of each region using

$$\tan(\theta_c) = \frac{x_c}{t_c} = U_c. \tag{1}$$

$U_{c,l}$ and $U_{c,h}$ are normalised by the local mean streamwise velocity ($\overline{U}_{local}$) at $z = 0.15\delta$. Note that $\overline{U}_{local}$ at $z = 0.15\delta$ changes as t increases due to the growth in δ. Figure 7 shows the PDF of $U_{c,l}$ ($\triangledown$), and $U_{c,h}$ ($\triangle$) at $z = 0.15\delta$. This figure reveals that the convection velocities of low-speed structures are somewhat slower than the high-speed structures. The results are consistent with other convection velocity studies in the literature [2, 9]. The discrepancy between the two PDF shown in figure 7 suggests that the local convection velocity is related to the streamwise velocity fluctuations. In short, the convection velocity of structures at a fixed wall position appears to be associated with the sign of the velocity fluctuations. Further investigation of the convection velocity analysis on the large-scale events is required to confirm the results.

Conclusions

A time-resolved PIV experiment on a towed flat plate is described. The quality of the developing turbulent boundary layer formed on the plate is evaluated using the evolution of mean flow parameters. The results are in good agreement with the canonical flat plate ZPG turbulent boundary layer. A preliminary analysis of the convection velocity of low- and high-speed structures at a given fixed wall-position is computed and the tentative suggestion at this stage is that the local convection velocity of the structures is correlated with the sign of their streamwise fluctuations. Regions of negative fluctuation are found to convect slower than regions of positive fluctuation.

Acknowledgements

References

[1] Chauhan, K. A., Monkewitz, P. A. and Nagib, H. M., Criteria for assessing experiments in zero pressure gradient boundary layers., *Fluid Dynamics Research*, **41**, 2009, 021404.

[2] Chung, D. and McKeon, B. J., Large-eddy simulation of large-scale flow structures in long channel flow, *Journal of Fluid Mechanics*, **661**, 2010, 341–364.

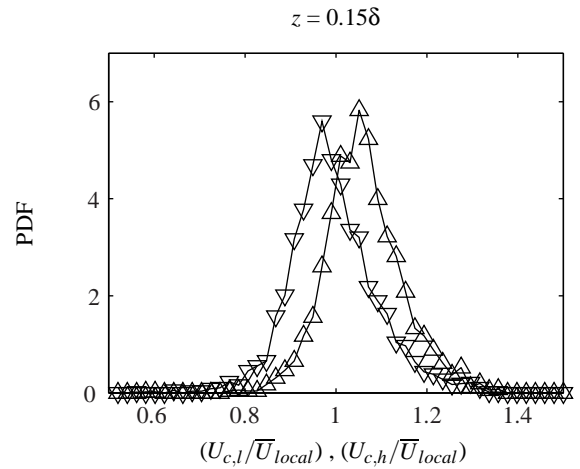[3] Clauser, F. H., The turbulent boundary layer, *Advances in Applied Mechanics*, **4**, 1956, 1–51.

Figure 7. PDF of convection velocities for negative instantaneous fluctuations $U_{c,l}$ ($\triangledown$) and for positive instantaneous fluctuations $U_{c,h}$ ($\triangle$) normalised by $\overline{U}_{local}$ at $z = 0.15\delta$

[4] Coles, D. E., The law of the wake in the turbulent boundary layer, *Journal of Fluid Mechanics*, **1**, 1956, 191–226.

[5] Collins, D. J., Coles, D. E. and Hicks, J. W., Measurements in the turbulent boundary layer at constant pressure in subsonic and supersonic flow. Part I. mean flow, Tech. Rep. 21, AEDC-TR-78, 1978.

[6] de Silva, C. M., Gnanamanickam, E. P., Atkinson, C., Buchmann, N. A., Hutchins, N., Soria, J. and Marusic, I., High spatial range velocity measurements in a high reynolds number turbulent boundary layer, *Physics of Fluids*, **26**, 2014, 025117.

[7] Erm, L. P. and Joubert, P. N., Low-Reynolds-number turbulent boundary layers, *Journal of Fluid Mechanics*, **230**, 1991, 1–44.

[8] Gao, Q., Ortiz-Dueñas, C. and Longmire, E. K., Evolution of coherent structures in turbulent boundary layers based on moving tomographic PIV, *Experiments in Fluids*, **54**, 2013, 1625.

[9] Lee, J., Lee, J. H., Choi, J. I. and Sung, H. J., Spatial organization of large- and very-large-scale motion in a turbulent channel flow, *Journal of Fluid Mechanics*, **749**, 2014, 818–840.

[10] Schlatter, P. and Örlü, R., Assessment of direct numerical simulation data of turbulent boundary layers, *Journal of Fluid Mechanics*, **659**, 2010, 116–126.